Alignment caused by photoionization and in radiative electron capture into excited states of hydrogenic high-Z ions

Jörg Eichler*
Bereich Theoretische Physik, Hahn-Meitner-Institut Berlin, D-14109 Berlin, Germany, and Fachbereich Physik, Freie Universität Berlin, D-14195 Berlin, Germany

A. Ichihara and T. Shirai
Japan Atomic Energy Research Institute, Tokai-mura, Ibaraki 319-11, Japan
(Received 8 April 1998)

In high-energy atomic collisions between bare high-Z projectiles and low-Z target atoms, an electron may be captured radiatively into the ground state or, alternatively, into an excited projectile state, which subsequently decays by x-ray emission. These processes are the inverse of a single-step or a two-step ionization, in which the first photon resonantly excites an electron from the hydrogenic $1s_{1/2}$ ground state and a second photon ionizes the excited electron. In this paper, we present a theoretical analysis with a particular emphasis on a detailed multipole decomposition of the photon wave function. This treatment is suitable for connecting angular correlations with alignment studies of the excited state. The anisotropy factors for angular correlations beween the beam axis and the decay x rays following radiative electron capture (REC) into the $2p_{3/2}$, $3p_{3/2}$, $3d_{3/2}$, and $3d_{5/2}$ levels of bare Xe^{54+}, Au^{79+}, Pb^{82+}, and U^{92+} projectiles with energies ranging from 10 MeV/u to 10 GeV/u are explicitly presented and the connection with the alignment is given. It is predicted that REC occurs predominantly into states with the minimal magnetic quantum number $\pm\frac{1}{2}$ indicating a strong alignment perpendicular to the beam axis. [S1050-2947(98)08609-0]

PACS number(s): 34.70.+e, 32.80.Fb

I. INTRODUCTION

In an energetic collision between a highly charged high-Z ion and a low-Z target atom, an electron may be captured by the projectile, while a simultaneously emitted photon carries away the excess energy and momentum. Since loosely bound target electrons can be considered as quasifree, the process is essentially the inverse of the photoelectric effect [1–3]. Recently, by studying relativistic atomic collisions with bare uranium ions, evidence has been found [4] for strong alignment of the intermediate state in two-step photoionization, in which the first photon resonantly excites the $1s_{1/2}$ ground state of U^{91+} to an intermediate $2p_{3/2}$ level and subsequently a second photon ionizes this state within its lifetime. In the (observed) inverse reaction, radiative electron capture (REC) occurs into the excited $2p_{3/2}$ level, which subsequently decays into the $1s_{1/2}$ ground state by emitting a Lyman-α_1 photon.

Since for high-Z projectiles and low-Z targets nonradiative capture is negligible at high collision energies, the detection of a $2p_{3/2}\rightarrow 1s_{1/2}$ decay photon in coincidence with the down-charged projectile is a clear indication of a two (or more) photon process [4]. The angular distribution of this photon with respect to the beam axis depends on the population of magnetic sublevels of the $2p_{3/2}$ excited state in the initial REC process. Its measurement provides the alignment and hence detailed information on the dynamics of the REC process, that is, equivalently, on the two-photon–one-electron ionization process.

In the present work we formulate the general theory of radiative electron capture into an excited state with subsequent decay by the emission of an x ray. We use an exact relativistic description of projectile and electron motion and include all multipoles in the expansion of the photon wave function. In the main part of the paper, for definiteness, we refer to the equivalent two-step photoionization. At the end, the results are expressed for REC. The aim of the present study is threefold. (a) We introduce an alternative formulation for photoionization, in which, from the outset, the electron direction is taken as quantization axis instead of the photon direction. This renders the multipole expansion of the photon wave more complicated, but yields results expressed in terms of alignment, i.e., of subshell occupation *probabilities* instead of *amplitudes*. (b) We derive the general anisotropy coefficient for the angular correlation between the emitted electron and the photon exciting the intermediate state and give the corresponding alignment parameter. (c) The general expressions for the anisotropy parameters are evaluated numerically for REC by Xe^{54+}, Au^{79+}, Pb^{82+}, and U^{92+} projectiles with energies between 10 MeV/u and 10 GeV/u, followed by electric dipole transitions $2p_{3/2}\rightarrow 1s_{1/2}$ or $3p_{3/2}\rightarrow 1s_{1/2}$ and by electric quadrupole transitions $3d_{3/2}\rightarrow 1s_{1/2}$ as well as $3d_{5/2}\rightarrow 1s_{1/2}$. This covers a wide range of presently possible experiments.

In Sec. II we introduce the notation, the necessary matrix elements, and density matrices by deriving the total cross section for photoionization. In Sec. III the differential cross section for single-step photoionization is given, while in Sec. IV the angular correlation for two-step photoionization is derived along with the corresponding correlations for radia-

*Electronic address: eichler@hmi.de

tive electron capture. In Sec. V numerical results are presented. Section VI contains some concluding remarks. Natural units $\hbar=m=c=1$ are used unless specified otherwise.

II. TOTAL CROSS SECTION FOR PHOTOIONIZATION

Let us assume that we have a single electron in the state $|\kappa_n\mu_n\rangle$ with the Dirac quantum number κ_n combining the angular momentum j_n with parity and the angular momentum projection μ_n. If the electron absorbs a photon with wave number $\mathbf{k}$ and circular polarization $\lambda=\pm1$, it may be emitted into a continuum state with momentum $\mathbf{p}$ and spin projection (on its own direction of propagation) $m_s=\pm\frac{1}{2}$.

While the direction of the photon is usually taken as the quantization axis [1–3,5], which provides a simple treatment of the photon wave function, we here adopt the direction of emission of the electron as quantization axis. This is, in fact, the natural choice for radiative recombination or REC, in which the accelerator beam defines the z axis.

The total cross section for photoionization is given by

$$\sigma^{\rm ph}=\frac{\alpha}{4k}\frac{1}{2j_n+1}\sum_{\mu_n}\frac{1}{2}\sum_{\lambda=\pm1}\int d\Omega_k \times\sum_{m_s=\pm\frac{1}{2}}|\langle\mathbf{p}m_s|\boldsymbol{\alpha}\cdot\hat{\mathbf{u}}_\lambda e^{i\mathbf{k}\cdot\mathbf{r}}|\kappa_n\mu_n\rangle|^2. \quad (1)$$

Since for radiative recombination and REC the direction of $\mathbf{p}$ is always fixed and well defined, it is meaningful to establish the partial cross sections for photoionization from a specific magnetic substate μ_n,

$$\sigma^{\rm ph}(\mu_n)=\frac{\alpha}{4k}\frac{1}{2}\sum_{\lambda=\pm1}\int d\Omega_k \times\sum_{m_s=\pm\frac{1}{2}}|\langle\mathbf{p}m_s|\boldsymbol{\alpha}\cdot\hat{\mathbf{u}}_\lambda e^{i\mathbf{k}\cdot\mathbf{r}}|\kappa_n\mu_n\rangle|^2. \quad (2)$$

Note that $\sigma^{\rm ph}(\mu_n)$ referring to the electron direction is *not* the usual quantity referring to the photon direction; see, e.g., [1–3,5]. In contrast, the present choice provides a more direct and useful interpretation as alignment; see Sec. IV. The partial cross sections (2) can also be expressed by the diagonal matrix elements of the density matrix $P^{\rm ph}_{\mu_n\mu_n'}$ as

$$\sigma^{\rm ph}(\mu_n)=\frac{\alpha}{4k}P^{\rm ph}_{\mu_n\mu_n}, \quad (3)$$

where the general density matrix for photoionization is

$$P^{\rm ph}_{\mu_n\mu_n'}=\frac{1}{2}\sum_{\lambda=\pm1}\int d\Omega_k\sum_{m_s}\langle\mathbf{p}m_s|\boldsymbol{\alpha}\cdot\hat{\mathbf{u}}_\lambda e^{i\mathbf{k}\cdot\mathbf{r}}|\kappa_n\mu_n\rangle \times\langle\mathbf{p}m_s|\boldsymbol{\alpha}\cdot\hat{\mathbf{u}}_\lambda e^{i\mathbf{k}\cdot\mathbf{r}}|\kappa_n\mu_n'\rangle^*. \quad (4)$$

A. Multipole and partial-wave expansion

For an arbitrary direction of incidence $\hat{\mathbf{k}}$ of the ionizing photon, the multipole decomposition of the photon wave is given by

$$\hat{\mathbf{u}}_\lambda e^{i\mathbf{k}\cdot\mathbf{r}}=\sqrt{2\pi}\sum_{L=1}^{\infty}\sum_{M=-L}^{M=L}i^L\sqrt{2L+1}\,\boldsymbol{\mathcal{A}}^{(\lambda)}_{LM}D^L_{M\lambda}(\hat{\mathbf{k}}\to\hat{\mathbf{z}}) \quad (5)$$

with the decomposition

$$\boldsymbol{\mathcal{A}}^{(\lambda)}_{LM}=\mathbf{A}_{LM}(m)+i\lambda\mathbf{A}_{LM}(e) \quad (6)$$

into the usual magnetic and electric multipole fields [6]. These fields can be expressed, respectively, as

$$\mathbf{A}_{LM}(m)=j_L(kr)\mathbf{T}^M_{LL},$$

$$\mathbf{A}_{LM}(e)=j_{L-1}(kr)\sqrt{\frac{L+1}{2L+1}}\mathbf{T}^M_{L,L-1}-j_{L+1}(kr)\sqrt{\frac{L}{2L+1}}\mathbf{T}^M_{L,L+1}, \quad (7)$$

where $j_l(kr)$ is a spherical Bessel function and the vector spherical harmonics $\mathbf{T}^M_{L\Lambda}$ are spherical tensors of rank L resulting from coupling the spherical unit vectors $\boldsymbol{\xi}_0=\hat{\mathbf{z}}$ and $\boldsymbol{\xi}_{\pm1}=\mp2^{-1/2}(\hat{\mathbf{x}}\pm i\hat{\mathbf{y}})$ with the spherical harmonics Y_{lm}, that is,

$$\mathbf{T}^M_{L\Lambda}=\sum_m\left(\begin{array}{cc|c}\Lambda & 1 & L\\ M-m & m & M\end{array}\right)Y_{\Lambda,M-m}\boldsymbol{\xi}_m. \quad (8)$$

Here the symbol (|) is the usual Clebsch-Gordan coefficient. Note that the parities of the magnetic and electric multipole fields $\boldsymbol{A}_{LM}(m,e)$ are $(-1)^L$ and $(-1)^{L+1}$, respectively.

Besides the photon waves, we also have to decompose the electronic continuum wave function of the final state into partial waves with Dirac quantum numbers $\kappa=\{j,l\}$, where l is the orbital angular momentum of the large component (while we use l' to denote the orbital angular momentum of the small component). Since we choose the electron momentum as the z axis, the expansion is simply given by [1]

$$|\mathbf{p}m_s\rangle=\sum_\kappa i^l e^{-i\Delta_\kappa}\sqrt{4\pi(2l+1)}\left(\begin{array}{cc|c}l & \frac{1}{2} & j\\ 0 & m_s & m_s\end{array}\right)\times\left(\begin{array}{c}g_\kappa(r)\chi^{m_s}_\kappa\\ if_\kappa(r)\chi^{m_s}_{-\kappa}\end{array}\right). \quad (9)$$

Here Δ_κ is the Coulomb phase shift, g_κ and f_κ are the radial wave functions of the upper and lower component, respectively, and $\chi^{m_s}_\kappa$ are the spin angular functions [6,1].

B. Matrix elements and density matrices

For a given initial state $|\kappa_n\mu_n\rangle$ and a specific partial wave $|\kappa m_s\rangle$, we can now calculate the exact relativistic magnetic and electric multipole matrix elements, respectively,

$$\langle \kappa m_s|\boldsymbol{\alpha}\cdot\mathbf{A}_{LM}(m)|\kappa_n\mu_n\rangle=\mathcal{T}_{LL}(\kappa m_s,\kappa_n\mu_n),$$

$$\langle \kappa m_s|\boldsymbol{\alpha}\cdot\mathbf{A}_{LM}(e)|\kappa_n\mu_n\rangle=\sqrt{\frac{L+1}{2L+1}}\mathcal{T}_{L,L-1}(\kappa m_s,\kappa_n\mu_n)-\sqrt{\frac{L}{2L+1}}\mathcal{T}_{L,L+1}(\kappa m_s,\kappa_n\mu_n), \tag{10}$$

so that from Eq. (6) the general multipole matrix element to be used in later expressions (17,19,20) is

$$\langle \kappa m_s|\boldsymbol{\alpha}\cdot\boldsymbol{\mathcal{A}}^{(\lambda)}_{LM}|\kappa_n\mu_n\rangle=\mathcal{T}_{LL}(\kappa m_s,\kappa_n\mu_n)+i\lambda\left[\sqrt{\frac{L+1}{2L+1}}\mathcal{T}_{L,L-1}(\kappa m_s,\kappa_n\mu_n)-\sqrt{\frac{L}{2L+1}}\mathcal{T}_{L,L+1}(\kappa m_s,\kappa_n\mu_n)\right]. \tag{11}$$

Owing to the different parity of the multipole fields, only the first term *or* the second will contribute in a matrix element between specified electronic states with well-defined parity. The general Dirac matrix element is

$$\begin{aligned}\mathcal{T}_{L\Lambda}(\kappa m_s,\kappa_n\mu_n)&=\langle \kappa m_s|j_\Lambda(kr)\boldsymbol{\alpha}\cdot\mathbf{T}^M_{L\Lambda}|\kappa_n\mu_n\rangle\\&=iU_\Lambda(\kappa,\kappa_n)\langle\chi^{m_s}_{\kappa}|\boldsymbol{\sigma}\cdot\mathbf{T}^M_{L\Lambda}|\chi^{\mu_n}_{-\kappa_n}\rangle\\&\quad-iV_\Lambda(\kappa,\kappa_n)\langle\chi^{m_s}_{-\kappa}|\boldsymbol{\sigma}\cdot\mathbf{T}^M_{L\Lambda}|\chi^{\mu_n}_{\kappa_n}\rangle,\end{aligned} \tag{12}$$

where in the second and third lines the matrix elements are reduced to the two-spinor space and the angular brackets now denote integration over the angular coordinates only, while the radial integrals are abbreviated as

$$U_\Lambda(\kappa,\kappa_n)=\int_0^\infty g_\kappa(r)j_\Lambda(kr)f_{\kappa_n}(r)r^2dr,$$
$$V_\Lambda(\kappa,\kappa_n)=\int_0^\infty f_\kappa(r)j_\Lambda(kr)g_{\kappa_n}(r)r^2dr. \tag{13}$$

Since the operator

$$\boldsymbol{\sigma}\cdot\mathbf{T}^M_{L\Lambda}=[\sigma\otimes Y_\Lambda]^M_L \tag{14}$$

is a spherical tensor operator of rank L acting in the spin and orbital space, one may decompose it into these subspaces by recoupling [7] to obtain the final result

$$\begin{aligned}&\mathcal{T}_{L\Lambda}(\kappa m_s,\kappa_n\mu_n)\\&=i\begin{pmatrix} j_n & L & j\\ \mu_n & M & m_s\end{pmatrix}\sqrt{\frac{3}{2\pi}}\sqrt{(2j_n+1)(2\Lambda+1)(2L+1)}\\&\quad\times\left[U_\Lambda(\kappa,\kappa_n)\sqrt{2l'_n+1}\begin{pmatrix} l'_n & \Lambda & l\\ 0 & 0 & 0\end{pmatrix}\begin{Bmatrix} l'_n & \frac12 & j_n\\ \Lambda & 1 & L\\ l & \frac12 & j\end{Bmatrix}\right.\\&\quad\left.-V_\Lambda(\kappa,\kappa_n)\sqrt{2l_n+1}\begin{pmatrix} l_n & \Lambda & l'\\ 0 & 0 & 0\end{pmatrix}\begin{Bmatrix} l_n & \frac12 & j_n\\ \Lambda & 1 & L\\ l' & \frac12 & j\end{Bmatrix}\right].\end{aligned} \tag{15}$$

In order to calculate the density matrix (4), we insert the expansion (5) and integrate over the directions of incidence of the photon. Using the relation [6]

$$\int D^{L'*}_{M'\lambda}D^L_{M\lambda}d\Omega_k=\frac{4\pi}{2L+1}\delta_{M'M}\delta_{L'L}, \tag{16}$$

we see that with the choice of the electron direction as the z axis, the density matrix becomes diagonal in M and hence in $\mu_n=m_s-M$.

The density matrix for photoionization then becomes

$$P^{\rm ph}_{\mu_n\mu'_n}=\delta_{\mu_n\mu'_n}16\pi^3\sum_\lambda\sum_{m_s}\sum_{L,M}\left|\sum_\kappa i^{-l}e^{i\Delta_\kappa}\sqrt{2l+1}\begin{pmatrix} l & \frac12 & j\\ 0 & m_s & m_s\end{pmatrix}\langle\kappa m_s|\boldsymbol{\alpha}\cdot\boldsymbol{\mathcal{A}}^{(\lambda)}_{LM}|\kappa_n\mu_n\rangle\right|^2. \tag{17}$$

Here the integration over the photon direction leads to an incoherent summation over the multipoles, while the electron partial waves are superimposed coherently. On the other hand, if we choose the photon direction as quantization axis, as is usually done [1], we have an incoherent sum over electron partial waves and a coherent summation over multipoles. The total μ_n-dependent cross section is obtained by inserting Eq. (17) into Eq. (3).

III. DIFFERENTIAL CROSS SECTION FOR PHOTOIONIZATION

The differential cross section for photoionization averaged over the initial substates μ_n is expressed by the diago-

nal elements of the density matrix as

$$\frac{d\sigma^{\rm ph}}{d\Omega}=\frac{\alpha}{4k}\frac{1}{2j_n+1}\sum_{\mu_n} P^{\rm ph}_{\mu_n\mu_n}(\hat{\mathbf{k}}) \tag{18}$$

in terms of the angle-dependent density matrix $P^{\rm ph}_{\mu_n\mu_n}(\hat{\mathbf{k}})$, which is obtained from Eq. (4) by discarding the integration over the photon direction. By inserting the expansion (5), we obtain

$$P^{\rm ph}_{\mu_n\mu_n}(\hat{\mathbf{k}})=\pi\sum_{\lambda}\sum_{m_s}\sum_{LL} i^{L-\bar{L}}\sqrt{(2L+1)(2\bar{L}+1)}$$
$$\times\langle \mathbf{p}m_s|\boldsymbol{\alpha}\cdot\boldsymbol{\mathcal{A}}^{(\lambda)}_{LM}|\kappa_n\mu_n\rangle\langle \mathbf{p}m_s|\boldsymbol{\alpha}\cdot\boldsymbol{\mathcal{A}}^{(\lambda)}_{LM}|\kappa_n\mu_n\rangle^*$$
$$\times D^{L}_{M\lambda}(\hat{\mathbf{k}}\rightarrow\hat{\mathbf{z}})D^{\bar{L}*}_{M\lambda}(\hat{\mathbf{k}}\rightarrow\hat{\mathbf{z}}), \tag{19}$$

where $M=\bar{M}=m_s-\mu_n$ is a fixed quantity. By combining the Wigner D matrices and inserting the partial-wave expansion of the electron continuum wave functions, we obtain

$$P^{\rm ph}_{\mu_n\mu_n}(\hat{\mathbf{k}})=4\pi^2\sum_{\nu} P_\nu(\cos\theta)\sum_{\lambda,m_s}\sum_{L,\bar{L}}(-1)^{M+1}i^{L-\bar{L}}\sqrt{(2L+1)(2\bar{L}+1)}\begin{pmatrix} L & \bar{L} & \nu\\ M & -M & 0\end{pmatrix}\begin{pmatrix} L & \bar{L} & \nu\\ \lambda & -\lambda & 0\end{pmatrix}$$
$$\times\sum_{\kappa,\bar{\kappa}} i^{-l+\bar{l}}e^{i(\Delta_\kappa-\Delta_{\bar{\kappa}})}\sqrt{(2l+1)(2\bar{l}+1)}$$
$$\times\begin{pmatrix} l & \frac{1}{2} & j\\ 0 & m_s & m_s\end{pmatrix}\begin{pmatrix} \bar{l} & \frac{1}{2} & \bar{j}\\ 0 & m_s & m_s\end{pmatrix}\langle\kappa m_s|\boldsymbol{\alpha}\cdot\boldsymbol{\mathcal{A}}^{(\lambda)}_{LM}|\kappa_n\mu_n\rangle\langle\bar{\kappa}m_s|\boldsymbol{\alpha}\cdot\boldsymbol{\mathcal{A}}^{(\lambda)}_{\bar{L}M}|\kappa_n\mu_n\rangle^*. \tag{20}$$

The matrix elements of the operator $\boldsymbol{\alpha}\cdot\boldsymbol{\mathcal{A}}^{(\lambda)}_{LM}$ are given by Eq. (11).

IV. ANGULAR CORRELATIONS IN TWO-STEP PHOTOIONIZATION

We now consider a two-step photoionization process in which a photon $\mathbf{k}',\lambda'$ excites an initial state $|\kappa_i,\mu_i\rangle$ to the intermediate state $|\kappa_n,\mu_n\rangle$ and a second photon $\mathbf{k},\lambda$ ionizes the intermediate state to the final Coulomb-distorted continuum state $|\mathbf{p},m_s\rangle$. Experimentally, this process is best implemented by its inverse [4]. This means that an electron $|\mathbf{p},m_s\rangle$ is radiatively captured into an excited projectile state $|\kappa_n,\mu_n\rangle$ with the simultaneous emission of a photon $\mathbf{k},\lambda$. Subsequently, the intermediate excited state decays into a lower state $|\kappa_i,\mu_i\rangle$, usually the ground state, by emitting another photon $\mathbf{k}',\lambda'$. Since the latter photon has a sharp well-known energy, it is easy to detect experimentally. If the REC photon $\mathbf{k},\lambda$ is not detected and the spin projections as well as the polarization of the decay photon are not observed, one obtains a simple angular correlation between the electron momentum $\mathbf{p}$ and the photon momentum $\mathbf{k}'$. Written for the corresponding two-step photoionization, the correlation is given by

$$W(\mathbf{p},\mathbf{k}')\propto\frac{1}{4}\sum_{\lambda,\lambda'=\pm1}\sum_{m_s,\mu_i}\int d\Omega_k$$
$$\times\left|\sum_{\mu_n}\langle\mathbf{p}m_s|\boldsymbol{\alpha}\cdot\hat{\mathbf{u}}_\lambda e^{i\mathbf{k}\cdot\mathbf{r}}|\kappa_n\mu_n\rangle\right.$$
$$\left.\times\langle\kappa_n\mu_n|\boldsymbol{\alpha}\cdot\hat{\mathbf{u}}_{\lambda'}e^{i\mathbf{k}'\cdot\mathbf{r}}|\kappa_i\mu_i\rangle\right|^2. \tag{21}$$

The correlation may now be expressed by density matrices

$$W(\mathbf{p},\mathbf{k}')\propto\sum_{\mu_n} P^{\rm ph}_{\mu_n\mu_n}(\hat{\mathbf{p}})P^{\rm ex}_{\mu_n\mu_n}(\hat{\mathbf{k}}'), \tag{22}$$

where $P^{\rm ph}_{\mu_n\mu_n'}(\hat{\mathbf{p}})$ is given by Eq. (4) and

$$P^{\rm ex}_{\mu_n'\mu_n}(\hat{\mathbf{k}}')=\frac{1}{2}\sum_{\lambda'=\pm1}\sum_{\mu_i}\langle\kappa_n\mu_n|\boldsymbol{\alpha}\cdot\hat{\mathbf{u}}_{\lambda'}e^{i\mathbf{k}'\cdot\mathbf{r}}|\kappa_i\mu_i\rangle$$
$$\times\langle\kappa_n\mu_n'|\boldsymbol{\alpha}\cdot\hat{\mathbf{u}}_{\lambda'}e^{i\mathbf{k}'\cdot\mathbf{r}}|\kappa_i\mu_i\rangle^*. \tag{23}$$

Since the excitation process connects two well-defined states, we may assume that only a single multipole-order K contributes. In most cases, it will be an electric dipole transition with $K=1$. The reduced multipole matrix element is a constant that can be factored out and discarded from the expression. Therefore,

$$\langle\kappa_n\mu_n|\boldsymbol{\alpha}\cdot\hat{\mathbf{u}}_{\lambda'}e^{i\mathbf{k}'\cdot\mathbf{r}}|\kappa_i\mu_i\rangle$$
$$\propto\begin{pmatrix} j_i & K & j_n\\ \mu_i & \mu_n-\mu_i & \mu_n\end{pmatrix}D^{K}_{\mu_n-\mu_i,\lambda'}(\hat{\mathbf{z}}\rightarrow\hat{\mathbf{k}}'). \tag{24}$$

Remembering that according to Eq. (17) the density matrix $P^{\rm ph}_{\mu_n\mu_n'}(\hat{\mathbf{p}})$ for photoionization becomes diagonal after integrating over the direction of photon propagation, we see that only the diagonal elements $P^{\rm ex}_{\mu_n\mu_n}(\hat{\mathbf{k}}')$ of the density matrix

for excitation enter into the angular correlation $W(\mathbf{p},\mathbf{k}')$. The diagonal density matrix hence becomes

$$P^{\rm ex}_{\mu_n\mu_n}(\hat{\mathbf{k}}') \propto \sum_{\mu_i,\lambda'} \begin{pmatrix} j_i & K & | & j_n \\ \mu_i & \mu_n-\mu_i & | & \mu_n \end{pmatrix}^2 \times D^K_{\mu_n-\mu_i,\lambda'}(\hat{\mathbf{z}}\to\hat{\mathbf{k}}') D^{K*}_{\mu_n-\mu_i,\lambda'}(\hat{\mathbf{z}}\to\hat{\mathbf{k}}'). \tag{25}$$

With the aid of the Clebsch-Gordan series, we express the product of two Wigner D-matrix elements by a sum over single D-matrix elements and subsequently we sum over the quantum numbers μ_i and λ', assuming that the photon polarization is not observed. As a result, we obtain

$$P^{\rm ex}_{\mu_n\mu_n}(\hat{\mathbf{k}}') \propto \sum_{\nu=0,\rm even}^{2K} (-1)^{1+j_n-\mu_n} \begin{pmatrix} j_n & j_n & | & \nu \\ \mu_n & -\mu_n & | & 0 \end{pmatrix} \times \begin{pmatrix} K & K & | & \nu \\ 1 & -1 & | & 0 \end{pmatrix} \begin{Bmatrix} j_n & K & j_i \\ K & j_n & \nu \end{Bmatrix} P_\nu(\cos\,\theta), \tag{26}$$

where $\{\ \}$ is a Wigner 6-j symbol, P_ν is a Legendre polynomial, and θ denotes the angle between the direction of the excitation photon $\mathbf{k}$ and the z axis, i.e., the direction of the emitted electron $\mathbf{p}$. If the circular photon polarization is detected, the odd Legendre polynomials will occur in addition to the even terms $\nu=0,2,\ldots$ in Eq. (26). Inserting Eq. (26) into Eq. (22), we obtain the angular correlation in the form

$$W(\theta) \propto \sum_{\nu=0,\rm even}^{2K} A_\nu P_\nu(\cos\,\theta), \tag{27}$$

with

$$A_\nu \propto \sum_{\mu_n} (-1)^{1+j_n-\mu_n} \begin{pmatrix} j_n & j_n & | & \nu \\ \mu_n & -\mu_n & | & 0 \end{pmatrix} \begin{pmatrix} K & K & | & \nu \\ 1 & -1 & | & 0 \end{pmatrix} \times \begin{Bmatrix} j_n & K & j_i \\ K & j_n & \nu \end{Bmatrix} \sigma^{\rm ph}(\mu_n), \tag{28}$$

where $\sigma^{\rm ph}(\mu_n)$ is the partial cross section for photoionization from the substate $|\kappa_n,\mu_n\rangle$ given by Eq. (3) and the diagonal density matrix (20). If we define the anisotropy coefficients as $\beta_{\nu 0}=A_\nu/A_0$, we can write

$$\beta_{\nu 0} = (2j_n+1)(2K+1) \begin{pmatrix} K & K & | & \nu \\ 1 & -1 & | & 0 \end{pmatrix} \begin{Bmatrix} j_n & K & j_i \\ K & j_n & \nu \end{Bmatrix} \times \frac{\sum_{\mu_n} (-1)^{j_i-\mu_n} \begin{pmatrix} j_n & j_n & | & \nu \\ \mu_n & -\mu_n & | & 0 \end{pmatrix} \sigma^{\rm ph}(\mu_n)}{\sum_{\mu_n} \sigma^{\rm ph}(\mu_n)}. \tag{29}$$

In addition to $\beta_{\nu 0}$, it is convenient to define the degree of alignment as [8–10]

$$\mathcal{A}_\nu = \frac{\sqrt{2j+1}}{\sum_\mu \sigma^{\rm ph}(\mu)} \sum_\mu (-1)^{j-\mu} \begin{pmatrix} j & j & | & \nu \\ \mu & -\mu & | & 0 \end{pmatrix} \sigma^{\rm ph}(\mu). \tag{30}$$

We now consider specific examples.

(i) In the particular case of dipole transitions between $j_n=3/2$ and $j_i=1/2$, Eq. (29) yields the anisotropy factor [4,8]

$$\beta_{20} = \frac{1}{2} \frac{\sigma^{\rm ph}(\frac{3}{2}) - \sigma^{\rm ph}(\frac{1}{2})}{\sigma^{\rm ph}(\frac{3}{2}) + \sigma^{\rm ph}(\frac{1}{2})} = \frac{1}{2}\mathcal{A}_2. \tag{31}$$

Here we have used only the positive angular momentum projections because $\sigma^{\rm ph}(\mu)=\sigma^{\rm ph}(-\mu)$. The factor β_{20} has been measured and calculated in Ref. [4]. Introducing the normalized probabilities $\mathcal{P}(\frac{1}{2})$ and $\mathcal{P}(\frac{3}{2})$ for populating the $j_n=1/2$ and $j_n=3/2$ states, respectively, with $\mathcal{P}(\frac{1}{2})+\mathcal{P}(\frac{3}{2})=1$, Eq. (31) leads to the result

$$\mathcal{P}(\tfrac{1}{2}) = \tfrac{1}{2} - \beta_{20}, \quad \mathcal{P}(\tfrac{3}{2}) = \tfrac{1}{2} + \beta_{20}. \tag{32}$$

(ii) For quadrupole transitions between $j_n=3/2$ and $j_i=1/2$, Eq. (29) yields the anisotropy factor

$$\beta_{20} = -\frac{1}{2} \frac{\sigma^{\rm ph}(\frac{3}{2}) - \sigma^{\rm ph}(\frac{1}{2})}{\sigma^{\rm ph}(\frac{3}{2}) + \sigma^{\rm ph}(\frac{1}{2})} = -\frac{1}{2}\mathcal{A}_2. \tag{33}$$

The corresponding relative population probabilities are

$$\mathcal{P}(\tfrac{1}{2}) = \tfrac{1}{2} + \beta_{20}, \quad \mathcal{P}(\tfrac{3}{2}) = \tfrac{1}{2} - \beta_{20}. \tag{34}$$

(iii) For quadrupole transitions between $j_n=5/2$ and $j_i=1/2$, one obtains the anisotropy factors

$$\beta_{20} = -\frac{1}{7} \frac{5\sigma^{\rm ph}(\frac{5}{2}) - \sigma^{\rm ph}(\frac{3}{2}) - 4\sigma^{\rm ph}(\frac{1}{2})}{\sigma^{\rm ph}(\frac{5}{2}) + \sigma^{\rm ph}(\frac{3}{2}) + \sigma^{\rm ph}(\frac{1}{2})} = -\sqrt{\frac{2}{7}}\mathcal{A}_2 \tag{35}$$

and

$$\beta_{40} = -\frac{2}{7} \frac{\sigma^{\rm ph}(\frac{5}{2}) - 3\sigma^{\rm ph}(\frac{3}{2}) + 2\sigma^{\rm ph}(\frac{1}{2})}{\sigma^{\rm ph}(\frac{5}{2}) + \sigma^{\rm ph}(\frac{3}{2}) + \sigma^{\rm ph}(\frac{1}{2})} = -\sqrt{\frac{8}{21}}\mathcal{A}_4. \tag{36}$$

The relative population probabilities, adding up to unity, in this case are given by

$$\mathcal{P}(\tfrac{1}{2}) = \tfrac{1}{3} + \tfrac{2}{3}\beta_{20} - \tfrac{1}{2}\beta_{40}, \quad \mathcal{P}(\tfrac{3}{2}) = \tfrac{1}{3} + \tfrac{1}{6}\beta_{20} + \tfrac{3}{4}\beta_{40}, \tag{37}$$

$$\mathcal{P}(\tfrac{5}{2}) = \tfrac{1}{3} - \tfrac{5}{6}\beta_{20} - \tfrac{1}{4}\beta_{40}.$$

Experimentally, photoionization of hydrogenlike high-Z ions is investigated via the inverse process of radiative recombination. The cross section $\sigma^{\rm RR}$ for radiative recombination is related by the principle of detailed balance to the cross section $\sigma^{\rm ph}$ for photoionization; see, e.g., [1]. The angle θ (still in the projectile frame) is replaced by its negative value, so that the even Legendre polynomials remain unchanged.

However, since radiative recombination in energetic collisions is detected in the laboratory frame, we have to transform the angular correlation from the projectile to the laboratory system [5], so that

$$W(\theta_{\rm lab}) \propto \frac{1}{\gamma^2(1-\beta\,\cos\,\theta_{\rm lab})^2}\left[1+\sum_{\nu=2,{\rm even}}^{2K}\beta_{\nu 0}P_\nu(\cos\,\theta)\right], \tag{38}$$

where

$$\cos\,\theta=\frac{\cos\,\theta_{\rm lab}-\beta}{1-\beta\,\cos\,\theta_{\rm lab}} \tag{39}$$

and the anisotropy parameters $\beta_{\nu 0}$ are inserted from Eq. (29) or from Eqs. (31)–(36).

V. RESULTS AND DISCUSSION

The preceding formulation differs from the standard treatment, in which the direction of the REC photon is taken as the quantization axis [1,2,5] and hence only multipoles with the angular momentum projection $\lambda=\pm 1$ can occur. While this simplifies the multipole expansion, one has to pay for it in the angular correlation by a *coherent* summation over multipole orders L and by a *coherent* summation over the magnetic substates μ_n of the intermediate atomic state. The latter fact precludes a formulation in terms of occupation probabilities, that is, in terms of alignment.

On the other hand, the treatment given here adopts the direction of the electron momentum (or the beam axis) as quantization axis. This leads to the general multipole expansion, but, in the angular correlation, to an *incoherent* summation over multipoles and, more importantly, to an *incoherent* summation over the magnetic substates μ_n of the intermediate atomic state. This allows for a formulation in terms of excitation probabilities and in terms of the degree of alignment $\mathcal{A}_\nu$.

Of course, both treatments lead to identical results, although the final formulas have very different appearances. Indeed, we checked numerically the identity of both approaches in a large number of cases including the results of [4]. This also provides a test of the computer program.

Since the exact numerical evaluation of the anisotropy parameters (29) and alignment parameters (30) is lengthy, we present the results for the experimentally most interesting cases in Figs. 1–4. The partial wave expansion for the relativistic electron wave function and the multipole expansion for the REC photon (which remains undetected) was carried to convergence. For the lowest projectile energies, it was necessary to include multipole orders up to $L=12$, while for the highest energies multipole orders typically up to $L=80$ had to be taken into account. In some cases of 10 GeV/u projectiles, even for $L=99$, the accuracy in the anisotropy parameter is only about 1%, whereas in all other cases it is by far better.

The angular distributions are symmetric about 90 ° in the projectile frame because they originate from the decay of a state with a definite parity. In particular, they are isotropic if the intermediate state has $j_n=\frac{1}{2}$, as it is the case for the Ly-α_2 $(2p_{1/2}\rightarrow 1s_{1/2})$ transition. Figure 1 shows the anisotropy

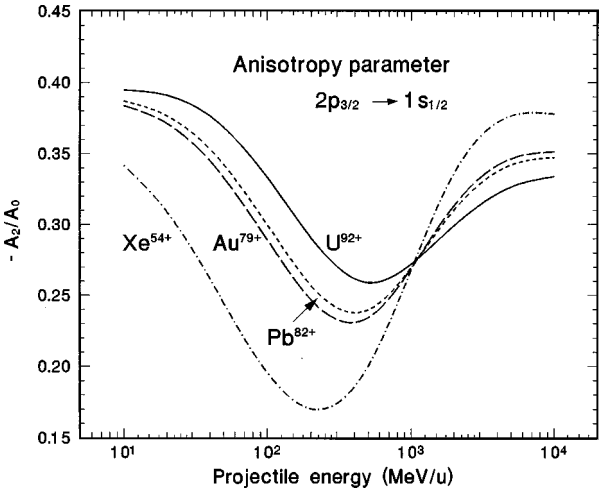

FIG. 1. *Negative* anisotropy parameter $-\beta_{20}=-A_2/A_0$ as a function of the projectile energy for the angular correlation between the beam direction and the $2p_{3/2}\rightarrow 1s_{1/2}$ dipole decay photon emitted after radiative electron capture into bare Xe, Au, Pb, and U projectiles.

of the electric dipole angular correlation between the Ly-$\alpha_1(2p_{3/2}\rightarrow 1s_{1/2})$ photon and an electron captured into the $2p_{3/2}$ state of the projectile (i.e., the beam direction), assuming that the REC photon is not observed. Note that the *negative* values of β_{20} are displayed. The results refer to bare xenon, gold, lead, and uranium projectiles with energies between 10 MeV/u and 10 GeV/u. In all cases, the anisotropy is largest for the lowest energy, has a minimum around 300 MeV/u, and becomes large again at higher energies. The theoretical results of [4] are included as special cases.

Figures 2–4 show the anisotropy coefficients for REC into the various M subshells. The dipole ($E1$) anisotropies for the transition $3p_{3/2}\rightarrow 1s_{1/2}$ plotted in Fig. 2 are similar to those of Fig. 1. Indeed, the only difference consists in the radial integrals for the $3p_{3/2}$ as compared to the $2p_{3/2}$ level and in the energy of the REC photon for a given projectile energy. The $3d_{3/2}$ and $3d_{5/2}$ states can decay to the $1s_{1/2}$ ground state only by an electric quadrupole ($E2$) transition. While the decay of the $3d_{3/2}$ state (see Fig. 3) still leads to an

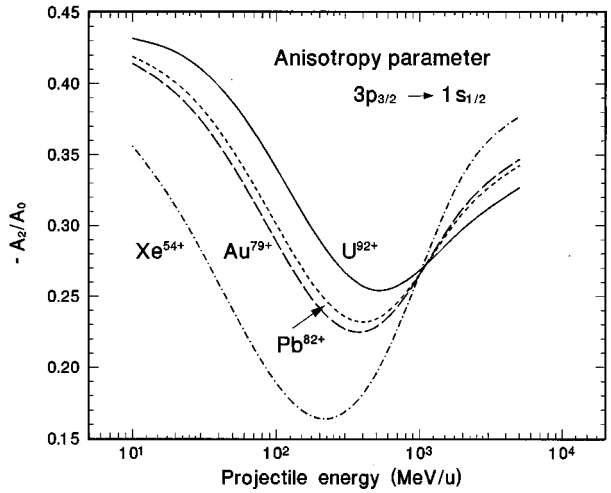

FIG. 2. Same as Fig. 1, but for capture into the $3p_{3/2}$ state.

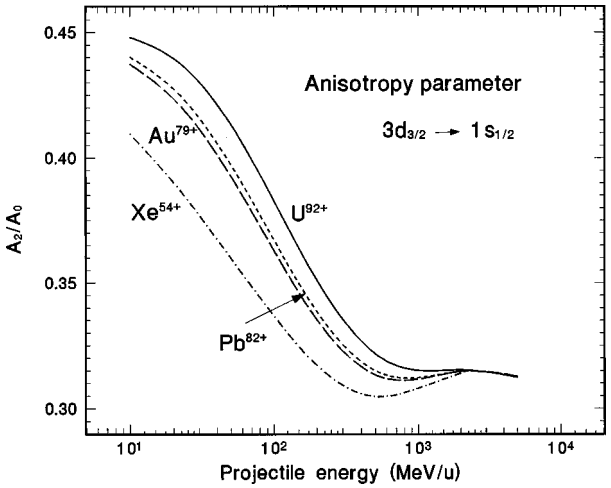

FIG. 3. Anisotropy parameter $\beta_{20}=A_2/A_0$ as a function of the projectile energy for the angular correlation between the beam direction and the $3d_{3/2}\rightarrow 1s_{1/2}$ quadrupole decay photon emitted after radiative electron capture into bare Xe, Au, Pb, and U projectiles.

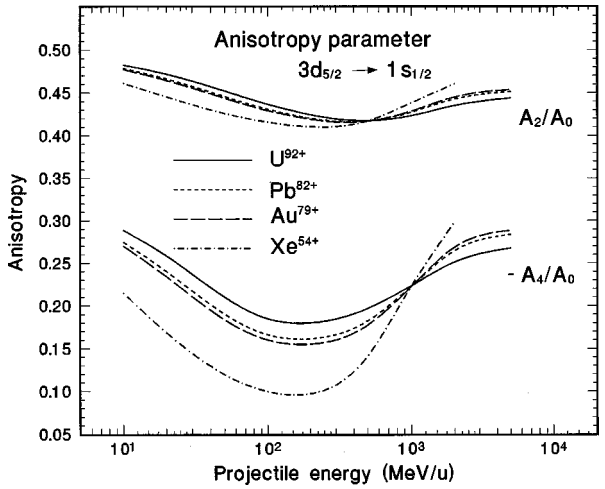

FIG. 4. Anisotropy parameters $\beta_{20}=A_2/A_0$ and $-\beta_{40}=-A_4/A_0$ as a function of the projectile energy for the angular correlation between the beam direction and the $3d_{5/2}\rightarrow 1s_{1/2}$ quadrupole decay photon emitted after radiative electron capture into bare Xe, Au, Pb, and U projectiles.

angular distribution (27) that contains only the zeroth and the second Legendre polynomial, the transition $3d_{5/2}\rightarrow 1s_{1/2}$ yields a more complicated angular distribution containing also the Legendre polynomial P_4 and hence the anisotropy coefficient β_{40}, in addition to β_{20} (see Fig. 4). The anisotropy parameters β_{20} for both quadrupole transitions are positive and have a behavior different from those of the dipole transitions of Figs. 1 and 2. In contrast, the anisotropy parameter β_{40} of Fig. 4 is negative and smaller.

In all cases (Figs. 1–4) we observe that the behavior of the anisotropy coefficient (or alignment) is qualitatively similar for all charge states from $Z=54$ to 92. The higher charge states give rise to larger alignments at lower energies and to smaller alignment at higher energies. In between, roughly at about 1 GeV/u, the anisotropy is independent of the charge state.

According to Eqs. (32), (34), and (37), the alignment parameters can be directly translated into relative population probabilities of the magnetic substates involved. In Table I we display the relative population probabilities (32) of the $\mu_n=\pm\frac{1}{2}$ and $\mu_n=\pm\frac{3}{2}$ states for REC into the $2p_{3/2}$ states of Xe^{54+}, Au^{79+}, Pb^{82+}, and U^{92+} as a function of the projectile energy. For this case, which is the most important one from the experimental point of view, it is seen that radiative electron capture occurs mainly into the states with $\mu_n=\pm 1/2$, indicating an alignment of the $j_n=3/2$ angular momentum perpendicular to the beam axis. Similar results can be inferred from Fig. 2 for the $3p_{3/2}$ state. This remarkably pronounced alignment, which comes about by a delicate energy-dependent balance of matrix elements in Eq. (4) or (17), implies a strongly linearly polarized Ly-α_1 radiation. From Eq. (34) for the $3d_{3/2}$ state and the *positive* sign of $\beta_{20}=A_2/A_0$ in Fig. 3 and, similarly, for the $3d_{5/2}$ state with the values and signs given in Fig. 4 and Eq. (37), we find again a predominant population of the $\mu_n=\pm\frac{1}{2}$ states and hence an alignment perpendicular to the beam direction. This is consistent with the classical picture that the orbital angular momentum transferred in a collision is directed perpendicular to the collision plane.

In an actual experiment, REC can also occur into highly excited states of the projectile. The excited electron will then cascade down, predominantly by electric dipole transitions, and eventually may end up in one of the intermediate states

TABLE I. Normalized probabilities $\mathcal{P}(\mu_n)$ for populating the magnetic substate $\pm\mu_n$ by REC into the $2p_{3/2}$ state of Xe^{54+}, Au^{79+}, Pb^{82+}, and U^{92+} for various projectile energies.

Energy	Xe^{54+}		Au^{79+}		Pb^{82+}		U^{92+}	
(MeV/u)	$\mathcal{P}(\pm\frac{1}{2})$	$\mathcal{P}(\pm\frac{3}{2})$	$\mathcal{P}(\pm\frac{1}{2})$	$\mathcal{P}(\pm\frac{3}{2})$	$\mathcal{P}(\pm\frac{1}{2})$	$\mathcal{P}(\pm\frac{3}{2})$	$\mathcal{P}(\pm\frac{1}{2})$	$\mathcal{P}(\pm\frac{3}{2})$
10	0.842	0.158	0.884	0.116	0.887	0.113	0.895	0.105
20	0.809	0.191	0.871	0.129	0.876	0.124	0.891	0.109
50	0.744	0.256	0.833	0.167	0.842	0.158	0.868	0.132
100	0.695	0.305	0.789	0.211	0.800	0.200	0.833	0.167
200	0.670	0.330	0.747	0.253	0.757	0.243	0.790	0.210
500	0.700	0.300	0.734	0.266	0.740	0.260	0.759	0.241
1000	0.768	0.232	0.769	0.231	0.769	0.231	0.772	0.228
2000	0.837	0.163	0.814	0.186	0.811	0.189	0.799	0.201
5000	0.877	0.123	0.846	0.154	0.842	0.158	0.826	0.174

considered here. While the cascade photons are usually not detected, the final decay from the L or M shell is measured by its specific decay energy. One expects that the contribution of undetected cascade transitions attenuates the angular measured distribution. This attenuation has been taken into account in [4] by using the GRASP code [11] for cascade feeding.

VI. CONCLUDING REMARKS

We have presented the general theoretical description of the angular distribution and the magnetic-substate population in the time-reversed process of photoionization in ion-atom collisions with a special emphasis on a detailed multipole decomposition of the photon wave function. The anisotropy of angular distributions of deexcitation x rays following REC into the sublevels of the L and M shells of high-Z projectiles at large nonrelativistic and at relativistic energies (from 10 MeV/u to 10 GeV/u) are explicitly given and displayed in Figs. 1–4. In all cases, the alignment parameter $\mathcal{A}_2$ shows significant negative values, while the alignment parameter $\mathcal{A}_4$ for the $3d_{5/2}\rightarrow 1s_{1/2}$ transition has a positive value. In all cases, the magnetic substates with $\mu_n=\pm\frac{1}{2}$ are predominantly populated, indicating a remarkable alignment perpendicular to the beam axis.

In order to compare with experimental data, one has to take into account the cascade feeding not included here. It turns out that at the energies for which measurements have been performed [4], the theoretical alignment is close to its minimum, so that for significantly smaller or larger energies, the anisotropy or the alignment is expected to considerably exceed the large alignment previously observed.

ACKNOWLEDGMENT

The authors benefitted from a long-standing collaboration with Th. Stöhlker, who pointed out to them the cases of experimental interest.

[1] For a summary of relativistic atomic collisions see, e.g., J. Eichler and W.E. Meyerhof, *Relativistic Atomic Collisions* (Academic, San Diego, 1995).

[2] A. Ichihara, T. Shirai, and J. Eichler, Phys. Rev. A **49**, 1875 (1994).

[3] J. Eichler, A. Ichihara, and T. Shirai, Phys. Rev. A **51**, 3027 (1995).

[4] Th. Stöhlker, F. Bosch, A. Gallus, C. Kozhuharov, G. Menzel, P. H. Mokler, H. T. Prinz, J. Eichler, A. Ichihara, T. Shirai, R. W. Dunford, T. Ludziejewski, P. Rymuza, Z. Stachura, P. Swiat, and A. Warczak, Phys. Rev. Lett. **79**, 3270 (1997).

[5] J. Eichler, Nucl. Phys. A **572**, 147 (1994).

[6] M. E. Rose, *Elementary Theory of Angular Momentum* (Wiley, New York, 1957).

[7] A. R. Edmonds, *Angular Momentum in Quantum Mechanics* (Princeton University Press, Princeton, 1957).

[8] E. G. Berezhko and N. M. Kabachnik, J. Phys. B **10**, 2467 (1977).

[9] K. Blum, *Density Matrix Theory and Applications* (Plenum, New York, 1981).

[10] N. Andersen, K. Bartschat, J. T. Broad, and I. V. Hertel, Phys. Rep. **279**, 251 (1997).

[11] K. Dyall *et al.*, Comput. Phys. Commun. **55**, 425 (1989).